Battery Cell Imbalance and Electric Vehicles Range: Correlation and NMPC-based Balancing Control

Jun Chen*, *Senior Member, IEEE* and Zhaodong Zhou
Department of Electrical and Computer Engineering
Oakland University
Rochester, MI 48309, USA
Email: {junchen,zhaodongzhou}@oakland.edu

2023 IEEE International Conference on Electro Information Technology (eIT) | 978-1-6654-9376-5/23/$31.00 ©2023 IEEE | DOI: 10.1109/EIT57321.2023.10187286

***Abstract*—Battery cell imbalance in electric vehicles (EV) has been extensively investigated in the literature to understand its origin and mitigation control. However, the correlation between cell imbalance and EV range deserves further investigation, which can be critical in designing a balancing controller. To address this issue, this paper conducts a Monte Carlo simulation to randomly sample cell parameters with different standard deviations to analyze their impacts. More specifically, distance correlation will be utilized to measure the correlation between battery cell parameters/variations and EV driving range. Furthermore, a nonlinear model predictive controller is developed to illustrate the efficacy of balancing controls in extending EV driving range.**

I. INTRODUCTION

Highly efficient battery systems are critical to electric vehicles and stationary smart grid applications [1]–[4]. One of the factors that limit battery performance is cell imbalance. Specifically, due to manufacturing and operation variations, battery cells can have different parameters, resulting in state-of-charge (SOC) imbalance during operations [5]. Such imbalance will in turn reduce the battery range and can potentially cause safety issues including thermal runaway [6]–[8].

Battery cell imbalance has been studied in literature to understand its impact on EV range [9], [10]. For example, [9] studies how the variations of initial SOC would impact EV range by using a synthetic speed profile. Furthermore, [10] simulates a simple battery model with heterogeneous cells, and performs a statistical analysis to understand the linear relationship between parameter variations and EV range. Alleviation strategies have also been proposed in literature to reduce the impact of battery cell imbalance [10]–[14]. However, existing literature has several limitations. First, the statistical analysis performed in [10] cannot capture nonlinear correlation between two variables, and since EV is a highly nonlinear system, the correlation between cell parameters and EV range can be nonlinear as well. Second, most of the control strategies proposed in literature are based on either rule-based control [15], simple feedback control [16], or linear model predictive control (MPC) [14], [17]. Exploitation on advanced control such as nonlinear MPC is not sufficiently studied yet.

To address these limitations, we conduct Monte Carlo simulation of EV with hundreds of connected battery cells to analyze how cell parameters and parameter variations impact EV driving range. Specifically, a real-world driving speed profile is used as vehicle reference speed, which is tracked by a detailed EV simulation model [10]. Distance correlation [18], [19], which can capture nonlinear correlation between two random variables and has value between 0 and 1, is utilized to measure the correlation between battery cell parameters and EV driving range. Moreover, in the first set of simulations, the battery is assumed to have identical cells, and we vary several key cell parameters to analyze their impacts. In the second set of simulations, the battery is assumed to have heterogeneous cells, each having different cell parameters (such as cell capacity, internal resistance, etc). Monto Carlo simulation is conducted to randomly sample those cell parameters with different standard deviations to analyze the impacts of cell variation level. Finally, a nonlinear MPC is developed to test its efficacy in extending EV driving range.

Compared to relevant literature [20]–[23], our work is different as we focus on analyzing nonlinear statistical correlation between battery cell parameters and EV driving range. Such quantification can then be insightful for balancing control design and only those parameters with statistical significance need to be explicitly addressed by battery management systems, and hence reducing the control complexity. Compared to [9] which only included speed profile variation, our work considers parameter variations at battery cell level. Furthermore, the battery model employed for simulation consists of over 100 heterogeneous cells, whereas [10] used an overly simplified battery model that has only 10 cells.

The rest of this paper is organized as follows. Section II discusses the simulation model of EV, while Section III briefly presents the necessary information for computing distance correlation. Section IV provides detailed results on the Monte Carlo simulation and discusses the impacts of battery cell parameter variations, and Section V presents the proposed nonlinear MPC balancing control algorithm and its performance. The paper is concluded in Section VI.

This work was supported in part by the faculty startup fund from School of Engineering and Computer Science at Oakland University and in part by National Science Foundation grant #2237317.

*Jun Chen is the corresponding author.

978-1-6654-9376-5/23/$31.00 ©2023 IEEE

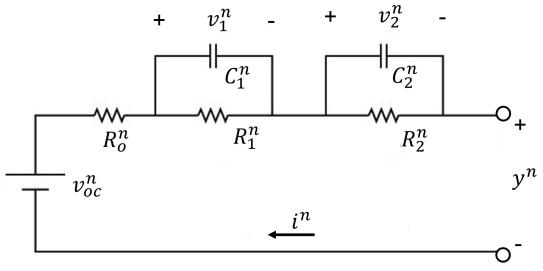

Fig. 1. Battery cell equivalent circuit model.

II. Simulation Model

A. Battery Dynamics

We consider a battery with P strings connected in parallel, each with S cells connected in series. The dynamics of cell n can be represented using an equivalent circuit model (ECM) [24]–[26], as follows,

$$\dot{s}^n = -\eta^n \frac{i^n}{3600 \times C^n} \tag{1a}$$

$$\dot{v}_1^n = -\frac{v_1^n}{R_1^n C_1^n} + \frac{i^n}{C_1^n} \tag{1b}$$

$$\dot{v}_2^n = -\frac{v_2^n}{R_2^n C_2^n} + \frac{i^n}{C_2^n} \tag{1c}$$

$$y^n = v_{oc}^n - v_1^n - v_2^n - i^n R_o^n. \tag{1d}$$

where s^n is the cell state-of-charge (SOC), v_1^n and v_2^n are relaxation voltages representing fast and slow transient dynamics, i^n is the cell current (where positive value indicates discharging), and y^n is the terminal voltage. Furthermore, v_{oc}^n is the open circuit voltage, η^n is the cell coulombic efficiency, and C^n is the cell Amp-Hour capacity. Finally, R_o^n, R_1^n, R_2^n, C_1^n and C_2^n are resistance and capacitance as shown in Fig. 1. Note that v_{oc}^n, R_o^n, R_1^n, R_2^n, C_1^n and C_2^n are all dependent on SOC s^n and cell temperatures T^n. See [26] for example of such dependency.

B. Electric Vehicle Propulsion Model

This section briefly describes the EV propulsion model used for simulation. Table I lists values for all model parameters related to EV propulsion systems that are fixed throughout the Monte Carlo simulation.

a) Vehicle speed control: In this work, the reference vehicle speed is taken from the TSDC dataset[1], provided by National Renewable Energy Laboratory [27], [28], which includes global positioning system (GPS) recording at an interval of 1 second. Fig 2 depicts the reference speed used for simulation. A PI speed controller is then used to control the requested battery power output to track the reference speed in Fig 2. The PI controller gains are fixed in all simulations to avoid any influence by the vehicle speed controller.

[1]Available at: https://www.nrel.gov/transportation/secure-transportation-data/. Accessed Sep. 15, 2021.

TABLE I
Parameters for the simulation models. Partiallydopted from [9].

Parameter	Unit	Physical Meaning	Value
m	kg	Car mass	1500
n_w	-	# of driving wheel	2
R	m	Effective wheel radius	0.2159
σ_b	rad	Bank angle	0
ρ	kg/m^3	Air density	1.225
C_d	-	Air drag coefficient	0.389
A_F	m^2	Front area	2
η_D	%	Propulsion efficiency	100
T_d	s	Propulsion time constant	0.3
B	-	Magic formula parameter	10
C	-	Magic formula parameter	1.9
D	-	Magic formula parameter	1
E	-	Magic formula parameter	0.97

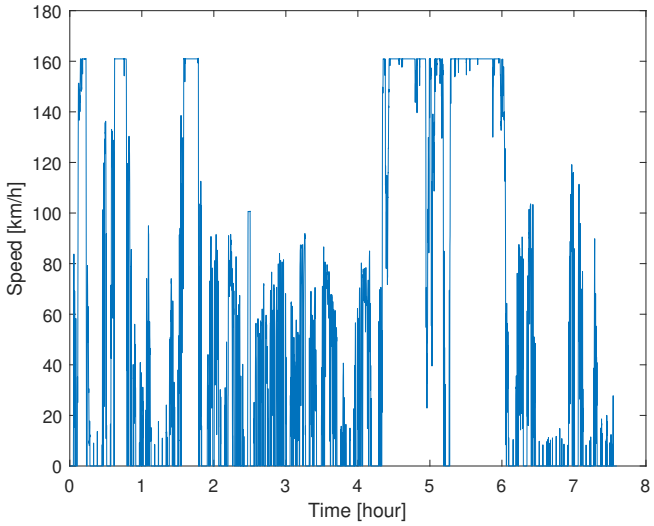

Fig. 2. Reference vehicle speed used for simulation.

b) Propulsion system dynamics: The EV propulsion systems consisting of electric motor, transmission, and final drive can be modeled as a first order transfer function [9], as follows,

$$G(s) = \frac{P_w}{P_b} = \frac{\eta_D}{T_d s + 1} \tag{2}$$

$$P_w = T\omega \tag{3}$$

where P_b is the actual battery power and P_w is the actual power delivered at the wheel, η_D is the overall propulsion efficiency, and T_d is the propulsion system time constant, T is the total driving torque as applied to driving wheels, and ω is the wheel angular speed.

c) Vehicle and wheel dynamics: The vehicle's longitudinal dynamics can be modeled as follow,

$$\dot{v}_x = \frac{n_w}{m} F_x - g \sin \sigma_b - \frac{1}{m} F_a \tag{4a}$$

$$\dot{\omega} = \frac{1}{I_w} \left(\frac{T}{n_w} - F_x R \right), \tag{4b}$$

where m is the vehicle mass, n_w is the number of driving wheels, σ_b is the road bank angle, I_w is the wheel rotational inertial, and F_x is the total tire force, as computed by the following Magic formula [29],

$$F_x = F_z D \sin \left\{ C \arctan \left[B s_r - E \left(B s_r - \arctan(B x) \right) \right] \right\}, \tag{5}$$

with F_z being normal force and s_r slip ratio defined as

$$s_r = \frac{\omega R - v_x}{v_x}. \tag{6}$$

Note that R here is the wheel effective radius.

d) Aerodynamic drag force: The aerodynamic drag force F_a in (5) can be calculated by [30]:

$$F_a = \frac{1}{2} \rho C_d A_F v_x^2, \tag{7}$$

where ρ is the air mass density, C_d is the aerodynamic drag coefficient, A_F is the effective front area. Note that here the wind speed is assumed to be 0.

III. Preliminary on Distance Correlation

Distance correlation will be used to measure the relationship between battery cell parameter variations and EV driving range. This section briefly presents the definition of distance correlation, together with the algorithm to compute sample distance correlation. For more details, please refer to [18], [19].

Given two random variables X and Y, the distance correlation between X and Y is defined as

$$dCor^2(X,Y) = \frac{dCov^2(X,Y)}{\sqrt{dVar^2(X) dVar^2(Y)}}, \tag{8}$$

where the squared distance covariance $dCov^2(X,Y)$ of X and Y is defined as

$$\begin{aligned} &dCov^2(X,Y) \\ &= \mathbb{E}\left[\|X - X'\| \, \|Y - Y'\|\right] + \mathbb{E}\left[\|X - X'\|\right] \mathbb{E}\left[\|Y - Y'\|\right] \\ &- \mathbb{E}\left[\|X - X'\| \, \|Y - Y''\|\right] - \mathbb{E}\left[\|X - X''\|\right] \mathbb{E}\left[\|Y - Y'\|\right] \end{aligned} \tag{9}$$

and the distance variance of X is given as

$$dVar^2(X) = dCov^2(X,X) \tag{10}$$

Given N samples X_n and Y_n, $n = 1, \ldots, N$ of random variables X and Y, Algorithms 1 and 2 compute the sample distance correlation between X_n and Y_n. In particular, Lines 2-7 calculate pairwise distance between samples, and Lines 10-19 compute sample distance covariance between X_n and Y_n. Algorithm 2 then implements (9) and (10) to compute sample distance correlation between X_n and Y_n.

Algorithm 1: Computing Sample Distance Covariance

Data: X_n and Y_n, $n = 1, \ldots, N$
Result: Sample distance covariance $dCov2$

1 Initialize A, B, C, D to be $N \times N$ matrices; initialize a and b to be vectors of length N;
2 **for** $n = 1, \ldots, N$ **do**
3 **for** $m = 1, \ldots, N$ **do**
4 $A(n,m) = \|X_n - X_m\|$;
5 $B(n,m) = \|Y_n - Y_m\|$;
6 **end**
7 **end**
8 $\bar{A} \leftarrow$ mean of all elements in A;
9 $\bar{B} \leftarrow$ mean of all elements in B;
10 **for** $n = 1, \ldots, N$ **do**
11 $a(n) \leftarrow$ the mean of nth row of A;
12 $b(n) \leftarrow$ the mean of nth row of B;
13 **end**
14 **for** $n = 1, \ldots, N$ **do**
15 **for** $m = 1, \ldots, N$ **do**
16 $C(n,m) = A(n,m) - a(n) - a(m) + \bar{A}$;
17 $D(n,m) = B(n,m) - b(n) - b(m) + \bar{B}$;
18 **end**
19 **end**
20 $dCov2 = \frac{1}{N^2} \sum_{n=1}^{N} \sum_{m=1}^{N} C(n,m) D(n,m)$;
21 **return** $dCov2$

Algorithm 2: Computing Sample Distance Correlation

Data: X_n and Y_n, $n = 1, \ldots, N$
Result: Sample distance Correlation $dCor2$

1 Compute sample distance covariance $dCov2$ of X and Y using Algorithm 1 with X_n and Y_n, $n = 1, \ldots, N$ as inputs;
2 Compute sample distance variance $dVar2X$ of X using Algorithm 1 with X_n and X_n, $n = 1, \ldots, N$ as inputs;
3 Compute sample distance variance $dVar2Y$ of Y using Algorithm 1 with Y_n and Y_n, $n = 1, \ldots, N$ as inputs;
4 $dCor2 \leftarrow dCov2 / \sqrt{dVar2X \times dVar2Y}$;
5 **return** $dCor2$

IV. Impacts of Cell Parameters and Imbalance

This section presents numerical results on the impacts of battery cell parameters, based on Monte Carlo simulation. In particular, two sets of simulations are performed. In the first set of simulations, the EV battery is assumed to have identical cells, with the cell parameters randomly generated. In the second set of simulations, the battery is assumed to have 108 heterogeneous cells, with the parameters of cell parameters being randomly generated. In other words, the first set of simulations analyzes the impact of battery cell parameters, while the second set of simulations focuses on the impacts

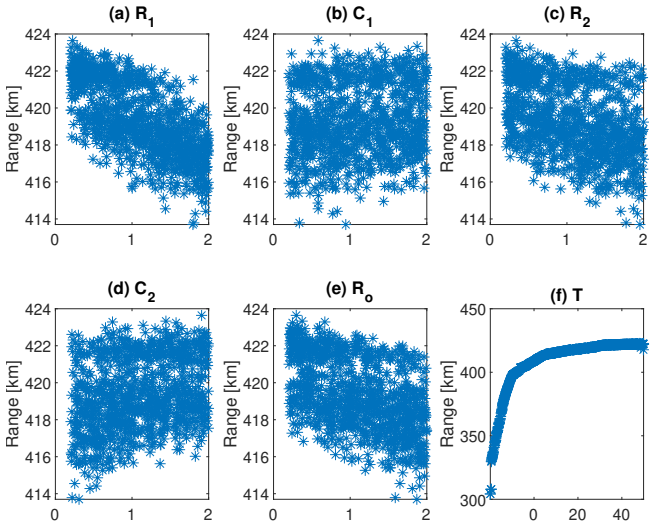

Fig. 3. Monte Carlo simulation results with identical cells.

of battery cell imbalance.

A. Results on Identical Cells

In this set of simulations, the EV battery is assumed to have identical cells. Recall that the cell ECM model (1) includes several parameters, e.g., cell capacity C^n, internal resistant R_1^n, R_2^n and R_o^n, capacitors C_1^n and C_2^n, and cell temperature T^n. Since it is intuitive that cell capacity C^n would have a significant impact on EV driving range, its value is fixed in all simulations.

We first randomly sample values for R_1, C_1, R_2, C_2, and R_o to be within 20%–200% of their respective nominal values. Fig. 3 (a)-(e) plot their impacts on EV driving range. We then fixed R_1, C_1, R_2, C_2, and R_o to their nominal value, and randomly sample cell temperature to be within -20^{o}C and 50^{o}C. Fig. 3 (f) plots the impacts of cell temperature on EV driving range. It can be seen that when batteries have identical cells, the temperature has the largest influence on the EV range. While the cell parameters do influence EV range, their impacts are relatively small compared to that of cell temperature. Table II (second column) lists the distance correlation of the cell parameters and EV driving range. It is then clear that internal resistant R_1^n, R_2^n and R_o^n can impact the EV range, while the range is almost independent of capacitors C_1^n and C_2^n. This is likely due to the fact that the capacitors only impact battery transient dynamics, and do not affect the DC resistance.

B. Results on Heterogeneous Cells

In this set of simulations, the EV battery is assumed to have heterogeneous cells. For each simulation, we first randomly generate values for C^n, R_1^n, C_1^n, R_2^n, C_2^n, and R_o^n with their nominal values as mean and a randomly sampled variance, run the simulation, and record the EV range. The whole process then repeats with another randomly sampled variance.

TABLE II
DISTANCE CORRELATION WHEN CELLS ARE IDENTICAL.

Parameter	Identical cells	Heterogeneous cells
C^n	-	0.906
R_1^n	0.422	0.003
C_1^n	0.007	0.005
R_2^n	0.159	0.001
C_2^n	0.064	0.001
R_o^n	0.205	0.002
T^n	0.741	0.691

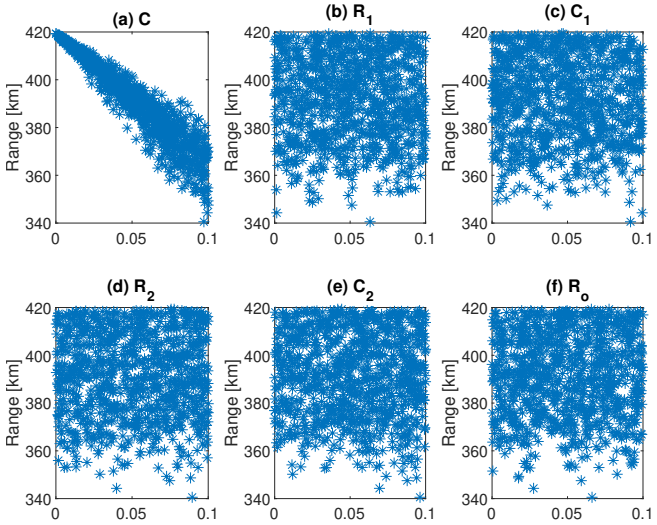

Fig. 4. Monte Carlo simulation results with heterogeneous cells.

Fig. 4 plots the impacts of cell imbalance on EV range. As can be seen, cell capacity variation seems to have the largest impact on the EV range. When the cells have 10% capacity compared to each other, the EV range can decrease from 420 km to around 340 km. For other parameters, it appears that there is no strong correlation between the EV range and the imbalance of internal resistance/capacitor. This can also be seen from the third column of Table II, where the cell imbalance of capacities has a distance correlation of 0.906 with EV driving range.

Finally, we assume all cells are different only by temperature T^n, and all the other parameters are fixed at their nominal values. For each simulation, we first randomly generate values for T^n with its nominal values as mean and a randomly sampled variance, run the simulation, and record the EV range. The whole process then repeats with another randomly sampled variance. The third column of Table II clearly indicates a strong correlation between cell temperature imbalance on EV driving range.

C. Additional Discussion

From these results, it is clear that C^n and T^n are the most important factors of EV driving range. When their nominal

value changes, even if there is no imbalance among cells, the EV driving range will be significantly changing as well. Moreover, even when their values are fixed, as long as there is an imbalance among cells, the EV range will be impacted. For example, by only exposing battery cells to different temperatures, EV driving range can be greatly decreased. On the other hand, for internal resistances R_1^n, R_2^n, and R_o^n, only their nominal value has a moderate impact on EV range, and the cell imbalance on these parameters does not have any implication on EV range. More specifically, connecting cells with larger internal resistance with cells with smaller internal resistance will not impact EV driving range, as long as the effective resistance is the same. Finally, for internal capacitors C_1^n and C_2^n, neither their nominal value nor their variance has any impact on EV driving range.

V. NMPC-BASED BALANCING CONTROL

In this section, we present a case study of using nonlinear model predictive control (NMPC) to perform battery cell balancing control. According to the discussion above, we only consider the cells to have imbalance on capacity C^n and assume that all the other parameters are at their nominal values.

A. NMPC-based Balancing Control

We consider the case that the battery is discharged under normal conditions and will stop discharge when the pack terminal voltage is lower than a cut-off voltage or pack SOC becomes 0. To extend the discharge time of the battery pack, it is necessary to add an appropriate balancing current to make all the cells' terminal voltage reach the cut-off voltage or SOC become 0 at the same time [8], [14]. To find a suitable balance current, here we use nonlinear model predictive control (NMPC). Similar to [14], the NMPC is set to track the SOC of all cells to follow a reference generated by using a nominal battery cell model. The optimal control problem (OCP) solved by MPC at each time step is shown as follows.

$$\min \quad J = \sum_{j=1}^{p} W_1 (s_{k+j}^n - s_{k+j}^r)^2 + W_2 u_k^2 \tag{11a}$$

$$\text{s.t.} \quad I_k = \frac{p_k}{y_{k-1}} \tag{11b}$$

$$\sum_{n=1}^{N} y^n \geq V_{\min} \tag{11c}$$

$$u_{\min} \leq u_k^n \leq u_{\max} \tag{11d}$$

$$\sum_{n=1}^{N} u_k^n = 0, \tag{11e}$$

where p is the prediction horizon, W_1 is the weight for output tracking error, W_2 is weight for manipulated variable, u_k here is the balancing current. Because our strategy in this report is dissipative balancing, the balancing current only transfers charge from one cell to another. Therefore, the sum of the balanced current needs to be equal to 0, which is reflected by the last constraint.

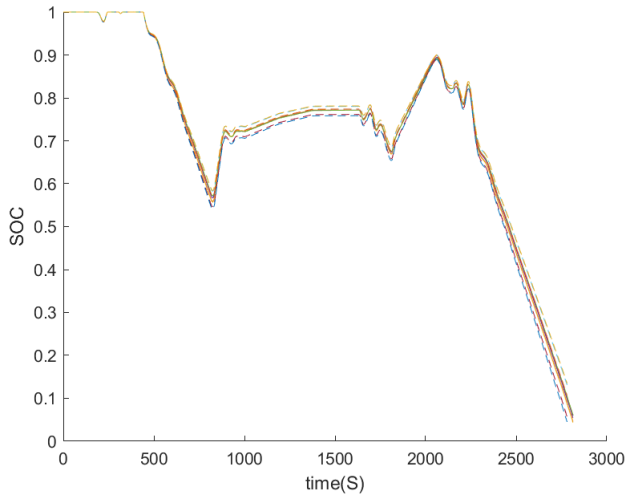

Fig. 5. SOC of each cell with MPC-based balancing (p=5) v.s. without balancing.

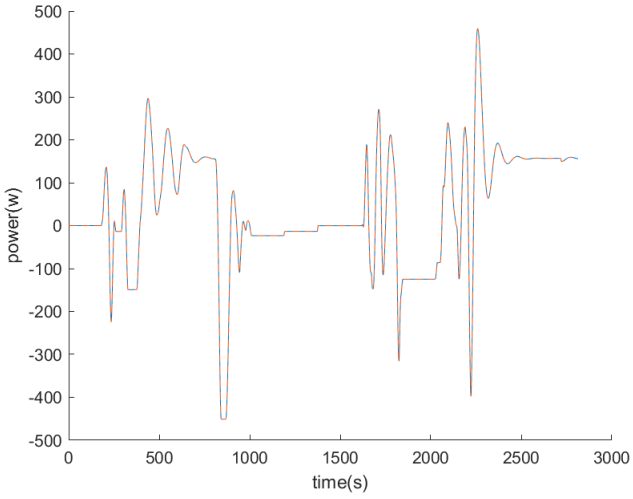

Fig. 6. Battery pack power with MPC-based balancing (p=5) v.s. without balancing.

B. Simulation Result

In this section, we will use simulations to find the effectiveness of NMPC on the battery system. A real driving cycle, i.e., FTP cycle, will be used as the driver requested power command to the battery. Furthermore, we randomly generated C^n to be within 10% deviation from the nominal values. To reduce simulation time, we consider a simple case of 5 cells connected in series, and we set the NMPC prediction horizon to $p = 5$.

Fig. 5 compares the SOC of each cell for the cases with and without NMPC balancing control. Fig. 6 compares the battery pack power for the cases with and without NMPC balancing control. As can be seen, though the battery pack provides similar traction power with and without balancing control, the cell SOCs with NMPC balancing control present lower variation, and hence the battery operation window is longer. In fact, without balancing control, the battery pack

stops operation after 2,781 seconds, while with balancing control, the battery operation time is 2,814 seconds. In other words, the range of battery operation is extended by 1%.

VI. CONCLUSION

This paper performed a statistical study to understand the correlation between battery cell imbalance and electric vehicle (EV) driving range, which can be critical in designing a balancing controller. In particular, a Monte Carlo simulation was conducted to randomly sample cell parameters with different standard deviations to analyze their impacts. Compared to existing work, a realistic battery model with 100 cells was used to conduct the simulation. Moreover, distance correlation was utilized to measure the nonlinear correlation between battery cell parameters/variations and EV driving range. Furthermore, a nonlinear model predictive controller (NMPC) was developed to illustrate the efficacy of balancing controls in extending EV driving range. Future work includes (1) further investigation of the NMPC-based balancing control to utilize all energy potential stored in EV battery packs, (2) application in other domains such as renewable energy [31], [32], as well as (3) design of power converter circuit for balancing [1], [33]

REFERENCES

[1] M. Kauer, S. Narayanaswamy, S. Steinhorst, M. Lukasiewycz, and S. Chakraborty, "Many-to-many active cell balancing strategy design," in *The 20th Asia and South Pacific Design Automation Conference*, Chiba, Japan, 2015, pp. 267–272.

[2] J. Chen, Z. Li, and X. Yin, "Optimization of energy storage size and operation for renewable-ev hybrid energy systems," in *2021 IEEE Green Technologies Conference*, Denver, CO, April 7–9, 2021.

[3] J. Chen and H. E. Garcia, "Economic optimization of operations for hybrid energy systems under variable markets," *Applied energy*, vol. 177, pp. 11–24, 2016.

[4] S. Sepasi, R. Ghorbani, and B. Y. Liaw, "A novel on-board state-of-charge estimation method for aged li-ion batteries based on model adaptive extended kalman filter," *Journal of Power Sources*, vol. 245, pp. 337–344, 2014.

[5] M. Dubarry, N. Vuillaume, and B. Y. Liaw, "Origins and accommodation of cell variations in li-ion battery pack modeling," *Int. J. of Energy Research*, vol. 34, no. 2, pp. 216–231, 2010.

[6] F. Hoekstra, H. J. Bergveld, and M. Donkers, "Range maximisation of electric vehicles through active cell balancing using reachability analysis," in *2019 American Control Conference (ACC)*, Philadelphia, PA, July 10-19, 2019, pp. 1567–1572.

[7] M. Einhorn, W. Roessler, and J. Fleig, "Improved performance of serially connected li-ion batteries with active cell balancing in electric vehicles," *IEEE Transactions on Vehicular Technology*, vol. 60, no. 6, pp. 2448–2457, 2011.

[8] F. S. Hoekstra, L. W. Ribelles, H. J. Bergveld, and M. Donkers, "Real-time range maximisation of electric vehicles through active cell balancing using model-predictive control," in *2020 American Control Conference*, Denver, CO, July 1–3, 2020, pp. 2219–2224.

[9] J. Chen, M. Liang, and X. Ma, "Probabilistic analysis of electric vehicle energy consumption using MPC speed control and nonlinear battery model," in *2021 IEEE Green Technologies Conference*, Denver, CO, April 7–9, 2021.

[10] J. Chen, Z. Zhou, Z. Zhou, X. Wang, and B. Liaw, "Impact of battery cell imbalance on electric vehicle range," *Green Energy and Intelligent Transportation*, vol. 1, no. 3, pp. 1–8, December 2022.

[11] Y. Shang, B. Xia, C. Zhang, N. Cui, J. Yang, and C. C. Mi, "An automatic equalizer based on forward–flyback converter for series-connected battery strings," *IEEE Transactions on Industrial Electronics*, vol. 64, no. 7, pp. 5380–5391, 2017.

[12] Y. Shang, N. Cui, and C. Zhang, "An optimized any-cell-to-any-cell equalizer based on coupled half-bridge converters for series-connected battery strings," *IEEE Transactions on Power Electronics*, vol. 34, no. 9, pp. 8831–8841, 2018.

[13] M. Preindl, "A battery balancing auxiliary power module with predictive control for electrified transportation," *IEEE Transactions on Industrial Electronics*, vol. 65, no. 8, pp. 6552–6559, 2017.

[14] J. Chen, A. Behal, and C. Li, "Active cell balancing by model predictive control for real time range extension," in *2021 IEEE Conference on Decision and Control*, Austin, TX, USA, December 13–15, 2021.

[15] J. Xu, B. Cao, S. Li, B. Wang, and B. Ning, "A hybrid criterion based balancing strategy for battery energy storage systems," *Energy Procedia*, vol. 103, pp. 225–230, 2016.

[16] C. Wang, G. Yin, F. Lin, M. P. Polis, C. Zhang, J. Jiang *et al.*, "Balanced control strategies for interconnected heterogeneous battery systems," *IEEE Transactions on Sustainable Energy*, vol. 7, no. 1, pp. 189–199, 2015.

[17] L. McCurlie, M. Preindl, and A. Emadi, "Fast model predictive control for redistributive lithium-ion battery balancing," *IEEE Transactions on Industrial Electronics*, vol. 64, no. 2, pp. 1350–1357, 2016.

[18] G. J. Székely, M. L. Rizzo, and N. K. Bakirov, "Measuring and testing dependence by correlation of distances," *The annals of statistics*, vol. 35, no. 6, pp. 2769–2794, 2007.

[19] G. J. Székely and M. L. Rizzo, "Brownian distance covariance," *The annals of applied statistics*, vol. 3, no. 4, pp. 1236–1265, 2009.

[20] Y. Hua, S. Zhou, H. Cui, X. Liu, C. Zhang, X. Xu, H. Ling, and S. Yang, "A comprehensive review on inconsistency and equalization technology of lithium-ion battery for electric vehicles," *International Journal of Energy Research*, vol. 44, no. 14, pp. 11 059–11 087, 2020.

[21] F. Feng, X. Hu, L. Hu, F. Hu, Y. Li, and L. Zhang, "Propagation mechanisms and diagnosis of parameter inconsistency within li-ion battery packs," *Renewable and Sustainable Energy Reviews*, vol. 112, pp. 102–113, 2019.

[22] C. Yang, X. Wang, Q. Fang, H. Dai, Y. Cao, and X. Wei, "An online soc and capacity estimation method for aged lithium-ion battery pack considering cell inconsistency," *Journal of Energy Storage*, vol. 29, p. 101250, 2020.

[23] X. Fan, W. Zhang, Z. Wang, F. An, H. Li, and J. Jiang, "Simplified battery pack modeling considering inconsistency and evolution of current distribution," *IEEE Transactions on Intelligent Transportation Systems*, vol. 22, no. 1, pp. 630–639, 2020.

[24] Z. Pei, X. Zhao, H. Yuan, Z. Peng, and L. Wu, "An equivalent circuit model for lithium battery of electric vehicle considering self-healing characteristic," *Journal of Control Science and Engineering*, vol. 2018, 2018.

[25] H. He, R. Xiong, X. Zhang, F. Sun, and J. Fan, "State-of-charge estimation of the lithium-ion battery using an adaptive extended kalman filter based on an improved thevenin model," *IEEE Transactions on Vehicular Technology*, vol. 60, no. 4, pp. 1461–1469, 2011.

[26] X. Lin, H. E. Perez, S. Mohan, J. B. Siegel, A. G. Stefanopoulou, Y. Ding, and M. P. Castanier, "A lumped-parameter electro-thermal model for cylindrical batteries," *Journal of Power Sources*, vol. 257, pp. 1–11, 2014.

[27] J. Fish, J. Gonder, V. Garikapati, J. Cappellucci, B. Borlaug, J. Holden, and L. Boyce, "Transportation secure data center," DOE Open Energy Data Initiative (OEDI); National Renewable Energy Laboratory, Tech. Rep., 2015. [Online]. Available: https://www.nrel.gov/transportation/secure-transportation-data/tsdc-drive-cycle-data.html

[28] J. Gonder, E. Burton, and E. Murakami, "Archiving data from new survey technologies: enabling research with high-precision data while preserving participant privacy," *Transportation Research Procedia*, vol. 11, pp. 85–97, 2015.

[29] E. Bakker, L. Nyborg, and H. B. Pacejka, "Tyre modelling for use in vehicle dynamics studies," *SAE Transactions*, pp. 190–204, 1987.

[30] R. Rajamani, *Vehicle dynamics and control*. Springer Science & Business Media, 2011.

[31] J. Chen and C. Rabiti, "Synthetic wind speed scenarios generation for probabilistic analysis of hybrid energy systems," *Energy*, vol. 120, pp. 507–517, 2017.

[32] J. S. Kim, J. Chen, and H. E. Garcia, "Modeling, control, and dynamic performance analysis of a reverse osmosis desalination plant integrated within hybrid energy systems," *Energy*, vol. 112, pp. 52–66, 2016.

[33] R. Badawi and J. Chen, "Enhancing enumeration-based model predictive control for dc-dc boost converter with event-triggered control," in *2022 European Control Conference*, London, UK, July 12–15, 2022.